Twist-Angle-Dependent Valley Polarization of Intralayer Moiré Excitons in van der Waals Superlattices

Renqi Wang,[1] Kai Chang,[2,3] Wenhui Duan,[1,4,5] Yong Xu,[1,5,6,*] and Peizhe Tang[7,8,†]
[1]State Key Laboratory of Low-Dimensional Quantum Physics and Department of Physics, Tsinghua University, Beijing 100084, China
[2]Center for Quantum Matter, Zhejiang University, Hangzhou 310058, China
[3]School of Physics, Zhejiang University, Hangzhou 310058, China
[4]Institute for Advanced Study, Tsinghua University, Beijing 100084, China
[5]Frontier Science Center for Quantum Information, Beijing 100084, China
[6]RIKEN Center for Emergent Matter Science (CEMS), Wako, Saitama 351-0198, Japan
[7]School of Materials Science and Engineering, Beihang University, Beijing 100191, China
[8]Max Planck Institute for the Structure and Dynamics of Matter, Center for Free Electron Laser Science, 22761 Hamburg, Germany

(Received 8 August 2024; revised 9 November 2024; accepted 18 December 2024; published 17 January 2025)

Twistronics, which utilizes the moiré potential to induce exotic excitations in twisted material systems, has garnered significant attention in recent years. In this Letter, using the Bethe-Salpeter calculations based on a continuum model of electronic structures, we explore the optical characteristics of intralayer moiré excitons in twisted bilayer transition metal dichalcogenide heterostructures. We find the Coulomb exchange interactions strongly influence these excitons and the degree of valley polarization and that the splitting between spin-singlet and spin-triplet moiré excitons can be effectively controlled by varying the twist angle. Specifically, intralayer bright spin-singlet moiré excitons confined in a twisted WSe_2/WS_2 heterostructure can achieve valley polarization levels as high as 90% at small twist angles, which holds promise for future applications in valleytronics. These findings underscore the twist angle as a novel parameter for manipulating the optical properties of moiré excitons, thereby establishing moiré semiconductors as a promising platform for investigating many-body physics in solid-state systems.

DOI: 10.1103/PhysRevLett.134.026904

Introduction—When two or more van der Waals layers with slight differences in lattice constant or orientation are aligned, long-scale structures called moiré superlattices can form in which many exotic phenomena have been observed, including correlated insulators [1–5], unconventional superconductivity [6–8], the quantum anomalous Hall effect [9–11], the fractional quantum anomalous Hall effect [11–15], and so on. As one of the most researched moiré systems, twisted bilayer transition metal dichalcogenides (TMDs) host the semiconducting moiré superlattices with strong spin-orbit coupling, in which excitons can be trapped by moiré potential [see Fig. 1(a)] [16–21], realizing moiré quantum emitter arrays [22]. Consequently, the moiré exciton formed in a TMD heterostructure not only preserves the spin-momentum locking effect, characteristic of a TMD monolayer, but also can be tuned by the new twisting degree of freedom, leading to the spatially varying selection rules [18,22,23], the long-sought boson crystal [22,24], and Mott-moiré excitons [25]. Such a moiré system serves as a new solid-state platform to simulate the problem in strong-correlation physics [4,25–27], indicating future optoelectronics applications [24,28,29].

In monolayer TMDs, the important role of the Coulomb exchange interactions, which can couple electronic states

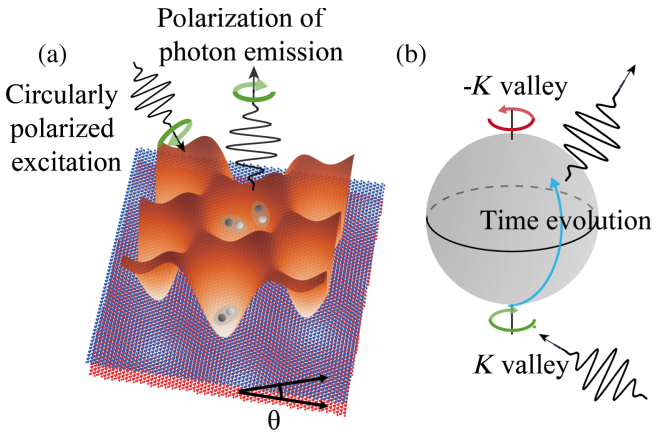

FIG. 1. (a) The schematic diagram of the moiré excitons trapped by the moiré potential. (b) The Bloch sphere represents the valley pseudospin of the lowest bright intralayer moiré exciton. The north and south poles correspond to valleys coupled with the left- and right-handed circularly polarized photons.

*Contact author: yongxu@mail.tsinghua.edu.cn
†Contact author: peizhet@buaa.edu.cn

from opposite valleys [30,31], has been well identified in optical spectroscopy [32,33]. Without such exchange coupling or other intervalley interactions [34–39], two valleys are decoupled and will host excitons with purely left- and right-handed circular polarization [23,40], which can be optically excited by photons with the same helicity [marked by the north and south poles in Fig. 1(b)]. The Coulomb exchange interactions can scatter excitons from one valley to the other, as illustrated by the diagrammatic trajectory of time evolution on the surface of the Bloch sphere in Fig. 1(b), thereby influencing valley polarization and dynamics, causing the valley depolarization, and hampering the future application of valleytronics [30–33,41,42]. The control and manipulation of valley polarization in optical excitations is one of the central topics for valleytronics in 2D materials and many efforts have been dedicated to this field [41,42]. Inspired by the promising development of twistronics [28], some spectral experiments have been conducted, which succeed in observing twist-angle-dependent behavior for the valley polarization in twisted TMD heterostructures [43]. On the other hand, the theoretical understanding of the role of exchange interactions in moiré semiconductors is still limited since the large-scale first-principles *GW*-Bethe-Salpeter equation (BSE) calculations [44,45] are too costly to consider exchange interactions in the study of finite momentum BSE calculations.

In previous studies, much theoretical research has used continuum models treating excitons in the moiré potential analogous to a Bloch problem [46,47], assuming that the moiré superlattice preserves the intrinsic nature of excitons [44]. In contrast to results from large-scale *GW*-BSE calculations for moiré excitons, such a treatment is an oversimplification and cannot properly describe the intralayer charge-transfer moiré excitons in twisted heterobilayer WSe_2/WS_2 [17,44]. To overcome this issue, we develop a distinct effective model that uses the moiré continuum Hamiltonian to describe the electronic properties in the moiré Brillouin zone (BZ) [26], then incorporate the Coulomb interaction to construct the BSE kernel matrix [45,48–53], and solve the BSE to obtain intralayer moiré excitons. Applying this method to a twisted WSe_2/WS_2 heterostructure, we observe optically active trapped moiré excitons and charge-transfer moiré excitons, consistent with results from large-scale *GW*-BSE calculations [44]. By varying the twist angle, the exciton binding energy and the valley polarization of the lowest bright moiré excitons can be manipulated efficiently. In addition to spin-singlet bright moiré excitons, we also study spin-triplet moiré excitons and find that the Coulomb exchange interactions play a significant role in the energy splitting between spin-singlet and triplet excitons, which varies with twist angles and could influence the dynamics of the moiré excitons. Our results indicate that the twist angle is a useful degree of freedom to control the valley depolarization of moiré excitons, and the ideal valley polarization can be realized in the twisted TMD with small twist angles.

Results—For definiteness, herein we consider the low-energy intralayer exciton of WSe_2 in the twisted WSe_2/WS_2 heterostructure, which is composed of the electron and hole in the same WSe_2 layer. The other layer, such as WS_2, provides the moiré potential through

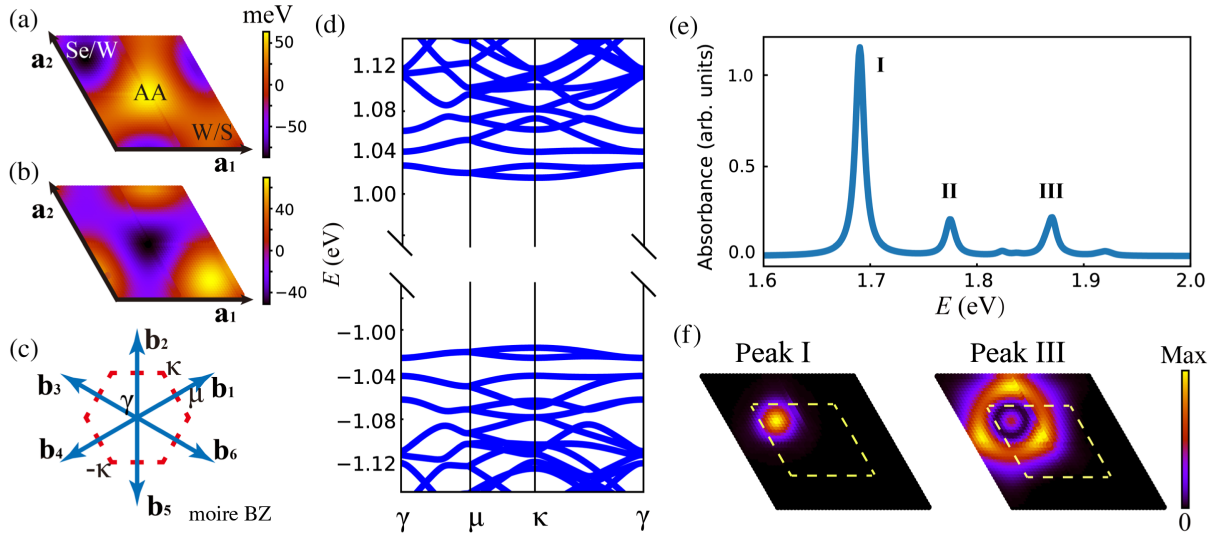

FIG. 2. (a),(b) The moiré potential fitted from the first-principles calculation for the valence band and conduction band, respectively. (c) The moiré Brillouin zone and the six lowest-order reciprocal lattice vectors. (d) The moiré band structure of WSe_2 calculated from the continuum model with $\theta = 2.5°$. The Fermi level is set as zero. (e) The absorbance spectrum of the WSe_2 intralayer moiré excitons in the twisted WSe_2/WS_2 correspondingly. (f) The real space distribution of the moiré exciton wave functions $|\Psi_{S,\mathbf{Q}=0}(\mathbf{r_e}, \mathbf{r_h})|^2$ for Peaks I and III as shown in (e). The area encircled by the yellow dashed line corresponds to the moiré unit cell in (a). The hole position is fixed at the Se/W region.

interlayer coupling. Consequently, the electronic properties of moiré systems that we focus on can be described by a two-band $\mathbf{k}\cdot\mathbf{p}$ Hamiltonian of WSe_2 [54], affected by a periodic moiré potential with the moiré period, $a_M \approx a_0/\theta$, where a_0 is the lattice constant of the monolayer WSe_2 and θ is the twist angle. The effective Hamiltonian has the form [55]

$$\hat{H}(\mathbf{k}) = \hbar v_F(\mathbf{k}-\mathrm{K})\cdot\boldsymbol{\sigma} + \frac{E_g}{2}\sigma_z + \Delta(\mathbf{r})$$
$$\Delta(\mathbf{r}) = \sum_j V_j \exp(i\mathbf{b}_j\cdot\mathbf{r}). \quad (1)$$

Herein, $\boldsymbol{\sigma}$ represents the pseudospin basis corresponding to the d orbitals of the W atoms, $\hbar$ is the reduced Planck's constant, v_F is the velocity parameter with $\hbar v_F = 3.9$ eV Å [54], and E_g stands for the direct band gap in monolayer WSe_2 with the value of 2.05 eV [44]. $\mathbf{b}$ is the reciprocal lattice vectors in moiré lattice, and $\Delta(\mathbf{r})$ is the moiré potential. Typically, this potential is approximated by the lowest Fourier expansion, including only six reciprocal lattice vectors [see Fig. 2(c)]. Constrained by the threefold rotational symmetry around the $\hat{z}$ axis and the requirement that $\Delta(\mathbf{r})$ be a real number, we have $V_1 = V_3 = V_5 = V_2^* = V_4^* = V_6^* = \mathrm{diag}(V_c e^{i\phi_c}, V_v e^{i\phi_v})$, resulting in only four parameters [26,55–57]. The continuum model above [see Eq. (1)] only represents an electronic structure near one K valley in the moiré BZ, under the time-reversal symmetry $\mathcal{T}$ we can obtain corresponding results for states near the $-K$ valley. The Coulomb exchange interactions could couple these states at opposite valleys. From the first-principles calculations [see details in Supplemental Material (SM) [58]], we obtain $(V^c, \phi^c) = (12\ \mathrm{meV}, -136°)$ and $(V^v, \phi^v) = (15\ \mathrm{meV}, -45°)$, which are comparable with results reported in previous work [57]. In Figs. 2(a) and 2(b), we plot the moiré potentials in the moiré lattice for the valence band and conduction band, respectively, and the calculated electronic band structure from the continuum model is shown in Fig. 2(d). These results are qualitatively consistent with those calculated from large-scale GW calculations [44].

We numerically solve the moiré exciton BSE to obtain eigenenergy $\Omega^S_{\mathbf{Q}}$ and wave functions $\Psi_{S\mathbf{Q}}(\mathbf{r_e}, \mathbf{r_h})$ for moiré excitons based on the electronic structure from the continuum model (see details in SM [58]), where S represents the index of the excitons, $\mathbf{Q}$ is the center-of-mass momentum of the excitons, $\mathbf{r_e}$ and $\mathbf{r_h}$ are the positions of the composite electron and hole, respectively. Considering the magnitude of the wave vector of the light is much smaller than the size of moiré BZ, we first focus on the bright spin-singlet moiré excitons in the light cone ($\mathbf{Q} \sim 0$), which are composed of electron-hole pairs within the same continuum model of either the K or $-K$ valley [see Fig. 3(b) and SM [58]]. Once electrons and holes originate from the opposite untwisted valleys, they can compose the spin-triplet dark moiré excitons (see details in SM [58]) as a result of the spin-valley locking in untwisted TMD materials. Figure 2(e) shows the simulated absorption spectra for twisted WSe_2/WS_2 with $\theta = 2.5°$ (see details in SM [58]). Three optically active exciton peaks can be observed, corresponding to two trapped intralayer moiré excitons (Peaks I and II) and charge-transfer moiré excitons (Peak III). Herein, the moiré potential strongly modifies electronic states to form the moiré band, resulting in emergent exciton peaks [16,17,44]. The corresponding real-space exciton wave functions $|\Psi_{S,\mathbf{Q}=0}(\mathbf{r_e}, \mathbf{r_h})|^2$ for Peaks I and III are shown in Fig. 2(f). The lowest exciton resembles the isotropic hydrogen wave function with a radius much smaller than the moiré lattice constant a_M. In contrast, the distribution of exciton III is anisotropic and demonstrates characteristics of charge-transfer excitons [44]. Our results are qualitatively consistent with those calculated from large-scale GW-BSE calculations [44] in contrast to that from the exciton continuum model [46,47].

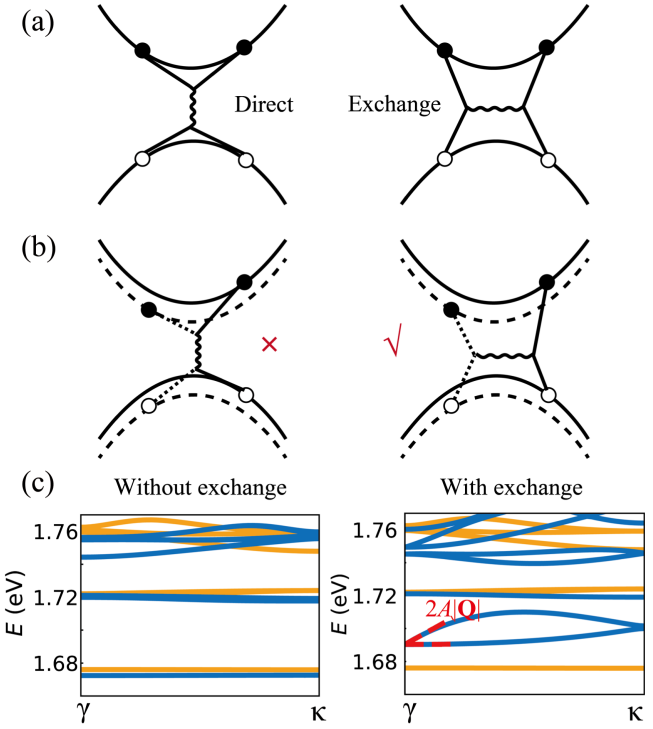

FIG. 3. (a), (b) The schematic diagram of the direct Coulomb interactions and exchange interactions between electron-hole pairs of the electronic continuum model (a) within the same valley and (b) near two opposite valleys. The solid line (K) and dashed line ($-K$) in (b) represent two different valleys, respectively. Only the exchange interactions couple the electronic state at two different valleys. (c) The band structure of the moiré exciton at $\theta = 2.5°$ without (left panel) and with (right panel) exchange interactions. The blue and yellow lines represent spin-singlet and spin-triplet moiré excitons, respectively. The red dashed line is fitted by the effective two-band exciton Hamiltonian.

To further explore the role of exchange interactions in the dispersion of moire excitons, we calculate the band structure of the moiré exciton by solving the BSE for electron-hole pairs with finite momentum $\mathbf{Q}$. For the bright spin-singlet moiré excitons that can be detected directly in optical spectroscopy, the direct Coulomb interactions [see Fig. 3(a)] provide the attraction between an electron and a hole, but cannot couple electron-hole pairs at opposite valleys K and $-K$, since this process requires a virtual photon with a large wave vector [see Fig. 3(b)]. Therefore, without exchange interactions, the electron-hole pairs in opposite valleys are independent, making the calculated moiré exciton bands from different valleys nearly degenerate [see blue lines in Fig. 3(c)]. However, when the intervalley exchange interaction, where a virtual photon with a small wave vector annihilates and creates electron-hole pairs at different momenta, is included, the continuum models near the opposite valleys are coupled [see Fig. 3(b)], lifting this degeneracy of exciton bands near γ point in the moiré BZ (see details in SM [58]). In addition, we observe an energy splitting between the lowest spin-singlet and spin-triplet moiré excitons (triplet-singlet splitting) [see blue and yellow lines in Fig. 3(c)] as a result of the intravalley exchange interactions (see details in SM [58]).

Previous studies have reported a two-band effective Hamiltonian to describe this intervalley coupling in monolayer TMDs [30,45]. We use the same effective model to describe spin-singlet moiré excitons when focusing on 1s-bright exciton as the ground state [72]. In this model, as fitted results for moiré excitons shown in the right panel of Fig. 3(c), the splitting lower exciton band $\Omega_l(\mathbf{Q})$ displays a parabolic dispersion, while the upper band $\Omega_u(\mathbf{Q})$ exhibits a nonanalytic linear dispersion

$$\Omega_l(\mathbf{Q}) = \Omega_0 + \frac{\hbar^2}{2M_l'}Q^2$$
$$\Omega_u(\mathbf{Q}) = \Omega_0 + 2A|\mathbf{Q}| + \frac{\hbar^2}{2M_u'}Q^2, \quad (2)$$

where A is the constant representing the dominant order of the exchange coupling, $M_{l,u}'$ is the effective mass of moiré excitons for the lower or upper band and is also renormalized by the exchange interactions [45]. The intervalley coupling term $2A|\mathbf{Q}|$, can lead to many observable phenomena such as the valley depolarization and valley dynamics in monolayer TMDs [30,31].

In the moiré systems, not only can various electronic properties be manipulated by the twist angle between different layers [73,74], but also the twist angle can control properties of moiré excitons. For example, the triplet-singlet splitting can vary with twist angles and influence the exciton dynamics (see details in SM [58]). Herein, we mainly focus on the optically bright spin-singlet moiré excitons, whose binding energy and valley polarization also depend on the twist angle. The calculated band structures of moiré excitons with different twist angles are shown in Figs. 4(a)–4(c). As the twist angle changes, the properties

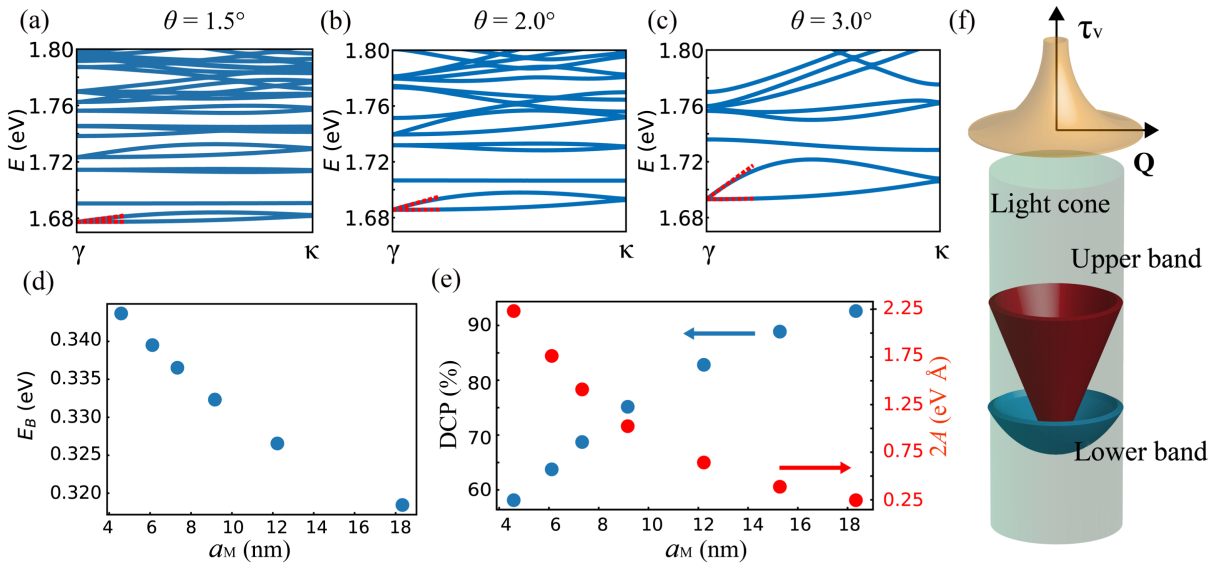

FIG. 4. (a)–(c) The WSe_2 intralayer moiré exciton band structures correspond to 1.5°, 2.0°, and 3.0° twisted WSe_2/WS2 heterobilayers, respectively. The red dashed lines represent the fitted results of the effective two-band exciton Hamiltonian. (d) The variation of the binding energy of the ground state moiré excitons with different twist angles. (e) The degree of circular polarization (DCP) and nonanalytic linear dispersion of the upper band $2A$ at different twist angles. (f) The schematic diagram of the dispersion of the lowest two moiré exciton bands in the light cone. The lower exciton band displays a parabolic dispersion, while the upper band exhibits a linear dispersion. Since the splitting between the two bands, which manifests the coupling between excitons from the two valleys, increases as the magnitude of momentum $|\mathbf{Q}|$ increases, the valley depolarization time $\tau_{v\mathbf{Q}}$ decreases with increasing $|\mathbf{Q}|$. The average of the valley depolarization time and estimation of the DCP is done in the light cone.

of moiré excitons change considerably. Quantitatively, we find that the binding energy of the ground state of moiré excitons (E^B) decreases as the twist angle decreases [see Fig. 4(d)]. We attribute this to the weaker Coulomb attraction between the electron and the hole in the larger moiré supercell. Since in the tight-binding limit, the kinetic energy of trapped moiré exciton [such as Peak I in Fig. 2(c)] scales with the superlattice constant as a_M^{-2}, while the Coulomb energy exceeds the kinetic energy at small twist angles and dominates the energy of the moiré excitons. On the other hand, both the on-site Coulomb interaction and the intersite Coulomb interaction decrease with the scale of the moiré superlattice, scaling as $a_M^{-1/2}$ and a_M^{-1}, respectively [57]. Therefore, the binding energy becomes weaker at smaller twist angles θ, correspondingly to the larger moiré lattice constants a_M [25].

To study the valley polarization of trapped moiré exciton, we perform calculations for intralayer moiré excitons in twisted WSe_2/WS_2 heterostructures with various twist angles and fit the coupling strength A at different angles including the exchange interactions [see Figs. 4(e) and 4(f)]. Our results demonstrate that the intervalley coupling induced by the exchange interactions sensitively depends on the twist angles in moiré systems. In the model study, the intervalley coupling through the exchange interactions is proportional to the probability density of exciton wave functions with the spatially overlapped electron and hole (approximately $A \propto |\Psi_{\mathbf{Q}=0}(\mathbf{r_e}=\mathbf{r_h},\mathbf{r_h})|^2$ [30,72]), and is hence inversely proportional to the square of the Bohr radius. The Bohr radius of trapped moiré exciton will increase with the moiré period when the twist angle decreases (see details in SM [58]), which also corresponds to the character of the variation of the binding energy. Therefore, the decrease of the twist angle will induce smaller coupling strength and a larger degree of circular polarization. For simplicity, we can estimate the rate of valley depolarization of exciton states with momentum $\mathbf{Q}$ [see Fig. 4(f)], which is proportional to the coupling strength A, and the circular polarization P (see details in SM [58]). For the typical recombination time ~1 ps for TMDs [75], the degree of circular polarization can vary from 60% to 90% by changing the moiré period in the range from 4 to 18 nm [see Fig. 4(e)]. Our calculation results are consistent with the experimental observation of intralayer moiré exciton in WS_2 for varying twist angles [43].

Conclusions—In this Letter, by solving the BSE based on the electronic continuum model, we systematically study the properties of intralayer moiré excitons in twisted WSe_2/WS_2 heterobilayers, revealing the important role of the exchange interactions for moiré excitons that was difficult to describe well in previous frameworks [44,46,47]. Varying the twist angle, we find the variations of the binding energy, the triplet-singlet splitting of moiré excitons, and the intervalley coupling strength for the lowest bright intralayer moiré excitons, indicating that valley polarization and other valleytronic properties in twisted TMDs associated with exchange interactions can be manipulated by adjusting the twist angle. The valley polarization as high as 90% can be achieved in twisted TMDs with small twist angles, supporting the future application of twisted TMD materials in valleytronics. Our results demonstrate that twisting is a useful degree of freedom to control the optical properties in moiré semiconductors, enabling novel functionalities in photoelectric moiré devices.

Acknowledgments—This work was supported by the National Key Basic Research and Development Program of China (Grant No. 2024YFA1409100), the Basic Science Center Project of NSFC (Grant No. 52388201), the National Natural Science Foundation of China (Grants No. 12334003, No. 12421004, and No. 12361141826), the National Key Basic Research and Development Program of China (Grant No. 2023YFA1406400), Innovation Program for Quantum Science and Technology (Grants No. 2023ZD0300500), and the National Science Fund for Distinguished Young Scholars (Grant No. 12025405). The calculations were performed at National Supercomputer Center in Tianjin using the Tianhe new generation supercomputer. P. T. was supported by the National Natural Science Foundation of China (Grants No. 12234011 and No. 12374053). K. C. was supported by the National Natural Science Foundation of China (NSFC) (Grant No. 92265203), and the Innovation Program for Quantum Science and Technology (Grant No. 2024ZD0300104).

[1] Y. Cao, V. Fatemi, A. Demir, S. Fang, S. L. Tomarken, J. Y. Luo, J. D. Sanchez-Yamagishi, K. Watanabe, T. Taniguchi, E. Kaxiras *et al.*, Correlated insulator behaviour at half-filling in magic-angle graphene superlattices, Nature (London) **556**, 80 (2018).

[2] Y. Xu, S. Liu, D. A. Rhodes, K. Watanabe, T. Taniguchi, J. Hone, V. Elser, K. F. Mak, and J. Shan, Correlated insulating states at fractional fillings of moiré superlattices, Nature (London) **587**, 214 (2020).

[3] E. C. Regan, D. Wang, C. Jin, M. I. Bakti Utama, B. Gao, X. Wei, S. Zhao, W. Zhao, Z. Zhang, K. Yumigeta *et al.*, Mott and generalized Wigner crystal states in WSe_2/WS_2 moiré superlattices, Nature (London) **579**, 359 (2020).

[4] Y. Tang, L. Li, T. Li, Y. Xu, S. Liu, K. Barmak, K. Watanabe, T. Taniguchi, A. H. MacDonald, J. Shan *et al.*, Simulation of Hubbard model physics in WSe_2/WS_2 moiré superlattices, Nature (London) **579**, 353 (2020).

[5] G. Chen, A. L. Sharpe, E. J. Fox, Y.-H. Zhang, S. Wang, L. Jiang, B. Lyu, H. Li, K. Watanabe, T. Taniguchi *et al.*, Tunable correlated Chern insulator and ferromagnetism in a moiré superlattice, Nature (London) **579**, 56 (2020).

[6] Y. Cao, V. Fatemi, S. Fang, K. Watanabe, T. Taniguchi, E. Kaxiras, and P. Jarillo-Herrero, Unconventional superconductivity in magic-angle graphene superlattices, Nature (London) **556**, 43 (2018).

[7] G. Chen, A. L. Sharpe, P. Gallagher, I. T. Rosen, E. J. Fox, L. Jiang, B. Lyu, H. Li, K. Watanabe, T. Taniguchi *et al.*, Signatures of tunable superconductivity in a trilayer graphene moiré superlattice, Nature (London) **572**, 215 (2019).
[8] L. Balents, C. R. Dean, D. K. Efetov, and A. F. Young, Superconductivity and strong correlations in moiré flat bands, Nat. Phys. **16**, 725 (2020).
[9] M. Serlin, C. Tschirhart, H. Polshyn, Y. Zhang, J. Zhu, K. Watanabe, T. Taniguchi, L. Balents, and A. Young, Intrinsic quantized anomalous Hall effect in a moiré heterostructure, Science **367**, 900 (2020).
[10] C.-Z. Chang, C.-X. Liu, and A. H. MacDonald, Colloquium: Quantum anomalous Hall effect, Rev. Mod. Phys. **95**, 011002 (2023).
[11] F. Xu, Z. Sun, T. Jia, C. Liu, C. Xu, C. Li, Y. Gu, K. Watanabe, T. Taniguchi, B. Tong *et al.*, Observation of integer and fractional quantum anomalous Hall effects in twisted bilayer $MoTe_2$, Phys. Rev. X **13**, 031037 (2023).
[12] Y. Xie, A. T. Pierce, J. M. Park, D. E. Parker, E. Khalaf, P. Ledwith, Y. Cao, S. H. Lee, S. Chen, P. R. Forrester *et al.*, Fractional Chern insulators in magic-angle twisted bilayer graphene, Nature (London) **600**, 439 (2021).
[13] Y. Zeng, Z. Xia, K. Kang, J. Zhu, P. Knüppel, C. Vaswani, K. Watanabe, T. Taniguchi, K. F. Mak, and J. Shan, Thermodynamic evidence of fractional Chern insulator in moiré $MoTe_2$, Nature (London) **622**, 69 (2023).
[14] J. Cai, E. Anderson, C. Wang, X. Zhang, X. Liu, W. Holtzmann, Y. Zhang, F. Fan, T. Taniguchi, K. Watanabe *et al.*, Signatures of fractional quantum anomalous Hall states in twisted $MoTe_2$, Nature (London) **622**, 63 (2023).
[15] H. Park, J. Cai, E. Anderson, Y. Zhang, J. Zhu, X. Liu, C. Wang, W. Holtzmann, C. Hu, Z. Liu *et al.*, Observation of fractionally quantized anomalous Hall effect, Nature (London) **622**, 74 (2023).
[16] K. L. Seyler, P. Rivera, H. Yu, N. P. Wilson, E. L. Ray, D. G. Mandrus, J. Yan, W. Yao, and X. Xu, Signatures of moiré-trapped valley excitons in $MoSe_2/WSe_2$ heterobilayers, Nature (London) **567**, 66 (2019).
[17] C. Jin, E. C. Regan, A. Yan, M. Iqbal Bakti Utama, D. Wang, S. Zhao, Y. Qin, S. Yang, Z. Zheng, S. Shi *et al.*, Observation of moiré excitons in WSe_2/WS_2 heterostructure superlattices, Nature (London) **567**, 76 (2019).
[18] K. Tran, G. Moody, F. Wu, X. Lu, J. Choi, K. Kim, A. Rai, D. A. Sanchez, J. Quan, A. Singh *et al.*, Evidence for moiré excitons in van der Waals heterostructures, Nature (London) **567**, 71 (2019).
[19] E. C. Regan, D. Wang, E. Y. Paik, Y. Zeng, L. Zhang, J. Zhu, A. H. MacDonald, H. Deng, and F. Wang, Emerging exciton physics in transition metal dichalcogenide heterobilayers, Nat. Rev. Mater. **7**, 778 (2022).
[20] K. F. Mak and J. Shan, Semiconductor moiré materials, Nat. Nanotechnol. **17**, 686 (2022).
[21] D. Huang, J. Choi, C.-K. Shih, and X. Li, Excitons in semiconductor moiré superlattices, Nat. Nanotechnol. **17**, 227 (2022).
[22] H. Yu, G.-B. Liu, J. Tang, X. Xu, and W. Yao, Moiré excitons: From programmable quantum emitter arrays to spin-orbit–coupled artificial lattices, Sci. Adv. **3**, e1701696 (2017).
[23] H. Yu, G.-B. Liu, and W. Yao, Brightened spin-triplet interlayer excitons and optical selection rules in van der Waals heterobilayers, 2D Mater. **5**, 035021 (2018).
[24] L. Du, M. R. Molas, Z. Huang, G. Zhang, F. Wang, and Z. Sun, Moiré photonics and optoelectronics, Science **379**, eadg0014 (2023).
[25] T.-S. Huang, Y.-Z. Chou, C. L. Baldwin, F. Wu, and M. Hafezi, Mott-moiré excitons, Phys. Rev. B **107**, 195151 (2023).
[26] F. Wu, T. Lovorn, E. Tutuc, and A. H. MacDonald, Hubbard model physics in transition metal dichalcogenide moiré bands, Phys. Rev. Lett. **121**, 026402 (2018).
[27] D. M. Kennes, M. Claassen, L. Xian, A. Georges, A. J. Millis, J. Hone, C. R. Dean, D. Basov, A. N. Pasupathy, and A. Rubio, Moiré heterostructures as a condensed-matter quantum simulator, Nat. Phys. **17**, 155 (2021).
[28] A. Ciarrocchi, F. Tagarelli, A. Avsar, and A. Kis, Excitonic devices with van der Waals heterostructures: Valleytronics meets twistronics, Nat. Rev. Mater. **7**, 449 (2022).
[29] J. C. Song and N. M. Gabor, Electron quantum metamaterials in van der Waals heterostructures, Nat. Nanotechnol. **13**, 986 (2018).
[30] H. Yu, G.-B. Liu, P. Gong, X. Xu, and W. Yao, Dirac cones and Dirac saddle points of bright excitons in monolayer transition metal dichalcogenides, Nat. Commun. **5**, 3876 (2014).
[31] T. Yu and M. W. Wu, Valley depolarization due to intervalley and intravalley electron-hole exchange interactions in monolayer MoS_2, Phys. Rev. B **89**, 205303 (2014).
[32] H. Yu, X. Cui, X. Xu, and W. Yao, Valley excitons in two-dimensional semiconductors, Natl. Sci. Rev. **2**, 57 (2015).
[33] G. Wang, A. Chernikov, M. M. Glazov, T. F. Heinz, X. Marie, T. Amand, and B. Urbaszek, Colloquium: Excitons in atomically thin transition metal dichalcogenides, Rev. Mod. Phys. **90**, 021001 (2018).
[34] C. Mai, A. Barrette, Y. Yu, Y. G. Semenov, K. W. Kim, L. Cao, and K. Gundogdu, Many-body effects in valleytronics: Direct measurement of valley lifetimes in single-layer MoS_2, Nano Lett. **14**, 202 (2014).
[35] R. Schmidt, G. Berghauser, R. Schneider, M. Selig, P. Tonndorf, E. Malic, A. Knorr, S. Michaelis de Vasconcellos, and R. Bratschitsch, Ultrafast Coulomb-induced intervalley coupling in atomically thin WS_2, Nano Lett. **16**, 2945 (2016).
[36] F. Mahmood, Z. Alpichshev, Y.-H. Lee, J. Kong, and N. Gedik, Observation of exciton–exciton interaction mediated valley depolarization in monolayer $MoSe_2$, Nano Lett. **18**, 223 (2018).
[37] Z. Lin, Y. Liu, Z. Wang, S. Xu, S. Chen, W. Duan, and B. Monserrat, Phonon-limited valley polarization in transition-metal dichalcogenides, Phys. Rev. Lett. **129**, 027401 (2022).
[38] H.-Y. Chen, D. Sangalli, and M. Bernardi, First-principles ultrafast exciton dynamics and time-domain spectroscopies: Dark-exciton mediated valley depolarization in monolayer WSe_2, Phys. Rev. Res. **4**, 043203 (2022).
[39] A. Kunin, S. Chernov, J. Bakalis, Z. Li, S. Cheng, Z. H. Withers, M. G. White, G. Schönhense, X. Du, R. K. Kawakami, and T. K. Allison, Momentum-resolved exciton coupling and valley polarization dynamics in monolayer WS_2, Phys. Rev. Lett. **130**, 046202 (2023).

[40] W. Yao, D. Xiao, and Q. Niu, Valley-dependent optoelectronics from inversion symmetry breaking, Phys. Rev. B **77**, 235406 (2008).
[41] J. R. Schaibley, H. Yu, G. Clark, P. Rivera, J. S. Ross, K. L. Seyler, W. Yao, and X. Xu, Valleytronics in 2D materials, Nat. Rev. Mater. **1**, 16055 (2016).
[42] S. A. Vitale, D. Nezich, J. O. Varghese, P. Kim, N. Gedik, P. Jarillo-Herrero, D. Xiao, and M. Rothschild, Valleytronics: Opportunities, challenges, and paths forward, Small **14**, 1801483 (2018).
[43] D. Dai, B. Fu, J. Yang, L. Yang, S. Yan, X. Chen, H. Li, Z. Zuo, C. Wang, K. Jin *et al.*, Twist angle-dependent valley polarization switching in heterostructures, Sci. Adv. **10**, eado1281 (2024).
[44] M. H. Naik, E. C. Regan, Z. Zhang, Y.-H. Chan, Z. Li, D. Wang, Y. Yoon, C. S. Ong, W. Zhao, S. Zhao *et al.*, Intralayer charge-transfer moiré excitons in van der Waals superlattices, Nature (London) **609**, 52 (2022).
[45] D. Y. Qiu, T. Cao, and S. G. Louie, Nonanalyticity, valley quantum phases, and lightlike exciton dispersion in monolayer transition metal dichalcogenides: Theory and first-principles calculations, Phys. Rev. Lett. **115**, 176801 (2015).
[46] F. Wu, T. Lovorn, and A. H. MacDonald, Topological exciton bands in moiré heterojunctions, Phys. Rev. Lett. **118**, 147401 (2017).
[47] F. Wu, T. Lovorn, and A. H. MacDonald, Theory of optical absorption by interlayer excitons in transition metal dichalcogenide heterobilayers, Phys. Rev. B **97**, 035306 (2018).
[48] G. Onida, L. Reining, and A. Rubio, Electronic excitations: Density-functional versus many-body Green's-function approaches, Rev. Mod. Phys. **74**, 601 (2002).
[49] M. Rohlfing and S. G. Louie, Excitonic effects and the optical absorption spectrum of hydrogenated Si clusters, Phys. Rev. Lett. **80**, 3320 (1998).
[50] M. Rohlfing and S. G. Louie, Electron-hole excitations and optical spectra from first principles, Phys. Rev. B **62**, 4927 (2000).
[51] F. Wu, F. Qu, and A. H. MacDonald, Exciton band structure of monolayer MoS_2, Phys. Rev. B **91**, 075310 (2015).
[52] M. O. Sauer, C. E. M. Nielsen, L. Merring-Mikkelsen, and T. G. Pedersen, Optical emission from light-like and particle-like excitons in monolayer transition metal dichalcogenides, Phys. Rev. B **103**, 205404 (2021).
[53] K. B. Simbulan, T.-D. Huang, G.-H. Peng, F. Li, O. J. Gomez Sanchez, J.-D. Lin, C.-I. Lu, C.-S. Yang, J. Qi, S.-J. Cheng *et al.*, Selective photoexcitation of finite-momentum excitons in monolayer MoS_2 by twisted light, ACS Nano **15**, 3481 (2021).
[54] D. Xiao, G.-B. Liu, W. Feng, X. Xu, and W. Yao, Coupled spin and valley physics in monolayers of MoS_2 and other group-VI dichalcogenides, Phys. Rev. Lett. **108**, 196802 (2012).
[55] J. Li, D. Zhai, C. Xiao, and W. Yao, Dynamical chiral Nernst effect in twisted van der Waals few layers, Quantum Front. **3**, 11 (2024).
[56] F. Wu, T. Lovorn, E. Tutuc, I. Martin, and A. H. MacDonald, Topological insulators in twisted transition metal dichalcogenide homobilayers, Phys. Rev. Lett. **122**, 086402 (2019).
[57] Y. Zhang, N. F. Q. Yuan, and L. Fu, Moiré quantum chemistry: Charge transfer in transition metal dichalcogenide superlattices, Phys. Rev. B **102**, 201115 (2020).
[58] See Supplemental Material, which includes Refs. [59–71], at http://link.aps.org/supplemental/10.1103/PhysRevLett.134.026904 for additional information on the details of the continuum model, the Bethe-Salpeter equations, the convergence tests of BSE calculations, spin-singlet and spin-triplet moiré excitons, as well as triplet-singlet splitting. The SM also includes an analysis of the exchange interaction and twist-angle-dependent Bohr radii of the Peak I moiré excitons.
[59] G. Kresse and J. Hafner, *Ab initio* molecular dynamics for liquid metals, Phys. Rev. B **47**, 558 (1993).
[60] G. Kresse and J. Furthmüller, Efficiency of *ab initio* total energy calculations for metals and semiconductors using a plane-wave basis set, Comput. Mater. Sci. **6**, 15 (1996).
[61] G. Kresse and J. Furthmüller, Efficient iterative schemes for *ab initio* total-energy calculations using a plane-wave basis set, Phys. Rev. B **54**, 11169 (1996).
[62] L. V. Keldysh, Coulomb interaction in thin semiconductor and semimetal films, Pis'ma Zh. Eksp. Teor. Fiz. **29**, 716 (1979) [JETP Lett. **29**, 658 (1979)], http://jetpletters.ru/ps/0/article_22207.shtml.
[63] A. Chernikov, T. C. Berkelbach, H. M. Hill, A. Rigosi, Y. Li, B. Aslan, D. R. Reichman, M. S. Hybertsen, and T. F. Heinz, Exciton binding energy and nonhydrogenic Rydberg series in monolayer WS_2, Phys. Rev. Lett. **113**, 076802 (2014).
[64] E. Mostaani, M. Szyniszewski, C. H. Price, R. Maezono, M. Danovich, R. J. Hunt, N. D. Drummond, and V. I. Fal'ko, Diffusion quantum Monte Carlo study of excitonic complexes in two-dimensional transition-metal dichalcogenides, Phys. Rev. B **96**, 075431 (2017).
[65] J. P. Perdew, K. Burke, and M. Ernzerhof, Generalized gradient approximation made simple, Phys. Rev. Lett. **77**, 3865 (1996).
[66] M. Szyniszewski, E. Mostaani, N. D. Drummond, and V. I. Fal'ko, Binding energies of trions and biexcitons in two-dimensional semiconductors from diffusion quantum Monte Carlo calculations, Phys. Rev. B **95**, 081301(R) (2017).
[67] M. Selig, G. Berghäuser, M. Richter, R. Bratschitsch, A. Knorr, and E. Malic, Dark and bright exciton formation, thermalization, and photoluminescence in monolayer transition metal dichalcogenides, 2D Mater. **5**, 035017 (2018).
[68] Y. Jiang, S. Chen, W. Zheng, B. Zheng, and A. Pan, Interlayer exciton formation, relaxation, and transport in TMD van der Waals heterostructures, Light Sci. Appl. **10**, 72 (2021).
[69] D. Y. Qiu, F. H. da Jornada, and S. G. Louie, Solving the Bethe-Salpeter equation on a subspace: Approximations and consequences for low-dimensional materials, Phys. Rev. B **103**, 045117 (2021).
[70] D. Schmitt, J. P. Bange, W. Bennecke, A. AlMutairi, G. Meneghini, K. Watanabe, T. Taniguchi, D. Steil, D. R. Luke, R. T. Weitz *et al.*, Formation of moiré interlayer excitons in space and time, Nature (London) **608**, 499 (2022).
[71] M. K. Man, J. Madéo, C. Sahoo, K. Xie, M. Campbell, V. Pareek, A. Karmakar, E. L. Wong, A. Al-Mahboob, N. S. Chan *et al.*, Experimental measurement of the intrinsic excitonic wave function, Sci. Adv. **7**, eabg0192 (2021).

[72] C. Li and W. Yao, Chiral excitonic systems in twisted bilayers from Förster coupling and unconventional excitonic Hall effects, Phys. Rev. B **110**, L121407 (2024).

[73] X.-W. Zhang, C. Wang, X. Liu, Y. Fan, T. Cao, and D. Xiao, Polarization-driven band topology evolution in twisted $MoTe_2$ and WSe_2, Nat. Commun. **15**, 4223 (2024).

[74] J. Yu, G. Jia, Q. Li, Y. Wang, K. Xiao, Y. Ju, H. Zhang, Z. Hu, Y. Guo, B. Lian, P. Tang, S. Zhou, Q.-K. Xue, and W. Li, Twist angle driven electronic structure evolution of twisted bilayer graphene, arXiv:2406.20040.

[75] K. F. Mak, K. He, J. Shan, and T. F. Heinz, Control of valley polarization in monolayer MoS_2 by optical helicity, Nat. Nanotechnol. **7**, 494 (2012).